

Upconversion Nanocrystals with High Lanthanide Content: Luminescence Loss by Energy Migration versus Luminescence Enhancement by Increased NIR Absorption

Alexandra Schroter, Susanne Märkl, Naomi Weitzel, and Thomas Hirsch*

Lanthanide-doped upconversion nanoparticles (UCNPs) have attracted a lot of interest due to their benefits in biological applications: They are not suffering from intermittence and provide nearly background-free luminescence. The progress in synthesis nowadays enables access to complex core-shell particles of controlled size and composition. Nevertheless, the frequently used doping ratio dates back to where mostly core-only particles of relatively large size have been studied. Especially at low power excitation as needed in biology, a decrease in particle size leads to a drastic decrease in the upconversion efficiency. An enhancement strategy based on an increased absorption rate of near-infrared light provided by an increase of the sensitizer content, together with the simultaneous blocking of the energy migration pathways to the particle surface, is presented. NaYbF₄(20%Er) particles of 8.5 nm diameter equipped with an about 2 nm thick NaYF₄ shell show significantly enhanced upconversion luminescence in the red (660 nm) compared to the most commonly used particles with only 20% Yb³⁺ and 2% Er³⁺. The impact of size, composition, and core-shell architecture on photophysical properties are studied. The findings demonstrate that an increase in doping rates enables the design of small, bright UCNPs useful for biological applications.

1. Introduction


Luminescent probes have established themselves as important reporters in biosensing and biomedicine, including organic dyes, fluorescent proteins, metal complexes, and semiconductor quantum dots.^[1–5] One promising class of luminescent probes are upconversion nanoparticles (UCNPs), which can overcome some drawbacks of common fluorophores. Those lanthanide-based nanocrystals absorb near-infrared (NIR) light and convert it into higher-energy visible or ultraviolet (UV) light.^[6–9] Since

the excitation lies in a wavelength range, where scattering and autofluorescence of biomolecules are very low, UCNPs allow deep tissue penetration and have the benefit of high signal-to-noise ratios additional to their photostability and sharp and tunable emission bands.^[10,11] The nanocrystals usually include a sensitizer–activator pair of lanthanide ions doped inside a NaYF₄ host lattice. The sensitizer absorbs NIR excitation light, transfers the energy of one, two, or three photons to the activator, which subsequently emits the upconversion luminescence.^[12,13] Many applications require strong upconversion to achieve high signal intensities and to keep the amount of nanoparticles in the organism low, which is why the high efficiency of the upconversion process is probably the most important issue when UCNPs are designed for biological applications.^[14,15] Several strategies such as energy harvesting, plasmonic enhancement, or triplet excited states in order to improve the

upconversion efficiency were already discussed in the literature.^[16–23] One essential strategy is the protection of the lanthanide ions from the environment by passivating the nanoparticle surface with a non-doped NaYF₄ shell. High energy vibrations of ligand or solvent molecules as well as crystal lattice defects, changing the local field around the lanthanides, lead to non-radiative decay processes that reduce the luminescence intensity.^[24] As shell growth enlarges the distance between the lanthanides and surface quenchers, strong increases of luminescence intensities and quantum yields can be achieved.^[24,25]

To increase the upconversion efficiencies one should also reconsider the content of sensitizer and activator ions. For many years (or decades), low doping of lanthanide ions inside nanocrystals was believed the best for efficient upconversion luminescence. To achieve green upconversion luminescence, the lanthanide doping inside a NaYF₄ crystal was once optimized to 18% Yb³⁺ (sensitizer ion) and 2% Er³⁺ (activator ion).^[13] The reason for the relatively low lanthanide concentrations is the theory of concentration quenching, where higher concentrations of lanthanide dopants lead to cross-relaxations between the ions as well as energy migration to surface quenchers—and hence reduced upconversion emission intensities.^[26,27] Even if the optimized composition was proposed for powders with crystals in the micrometer-range,

A. Schroter, S. Märkl, N. Weitzel, T. Hirsch
Institute of Analytical Chemistry
Chemo- and Biosensors
University of Regensburg
93040 Regensburg, Germany
E-mail: thomas.hirsch@ur.de

 The ORCID identification number(s) for the author(s) of this article can be found under <https://doi.org/10.1002/adfm.202113065>.

© 2022 The Authors. Advanced Functional Materials published by Wiley-VCH GmbH. This is an open access article under the terms of the Creative Commons Attribution-NonCommercial License, which permits use, distribution and reproduction in any medium, provided the original work is properly cited and is not used for commercial purposes.

DOI: 10.1002/adfm.202113065

these concentrations are still prominent for nanoparticle dispersions with diameters < 50 nm,^[26] where non-radiative decay processes on the surface become dominant, resulting in low upconversion efficiency.^[28] To compensate for the loss of luminescence caused by quenching processes, strategies emerged to increase the absorption cross-sections of the particles through higher lanthanide doping.^[29] It was found that concentration quenching can be overcome by high excitation power densities, since cross-relaxation and energy migration processes are hindered when all lanthanide ions are in excited state.^[27] Increasing the activator concentration with constant sensitizer concentration was demonstrated to lead to improved luminescence intensities.^[30,31] Similar results were achieved by increasing the Yb³⁺ concentration, where it was discovered that the higher the Yb³⁺ content, the higher are the luminescence intensities. High excitation power densities should be avoided for applications in living organisms,^[32] therefore it was a significant step when it was discovered, that not only high excitation power densities enable high lanthanide doping but also inert shell growth around the particles, which protects them from energy migration to surface quenchers.^[33–36] Core-shell structures with high lanthanide content were synthesized,^[37–39] which all showed improved luminescence intensities compared to similar particle architectures with lower lanthanide doping. One very promising approach was the synthesis of so-called “alloyed” nanocrystals by Cohen et al., where different Yb/Er ratios in a sodium lanthanide fluoride lattice equipped with a NaYF₄(20%Gd) shell were monitored at different power densities.^[40] They introduced alloyed UCNPs for low irradiance imaging, only composed of NaYbF₄ and NaErF₄ without the need for NaYF₄ as host lattice.

Enhancing the absorption of UCNPs is clearly beneficial for the upconversion performance, but higher lanthanide doping also facilitates energy transfer processes between the single ions due to decreasing ion-ion distances.^[41] While on the one hand energy migration can be useful, for example, for the transportation of energy across core-shell interfaces,^[42–49] it can on the

other hand strongly limit upconversion intensities. For example, NaErF₄ nanoparticles suffer from low luminescence intensities if they are not equipped with a NaYF₄ shell since the energy migrates through the crystal lattice until it gets quenched on the particle surface.^[34,50–53] The reduction of upconversion efficiency due to energy migration followed by surface quenching is an issue that should be valid for all systems with high concentrations of lanthanide ions. Consequently, it's unavoidable to get control over the energy migration and hinder the quenching processes to achieve bright luminescence.

Within this publication, the two main impacts of high lanthanide content in UCNPs will be discussed: higher absorption cross-sections on the one hand and increased energy migration between the lanthanide ions on the other hand. Ytterbium as sensitizer and erbium as activator ions were chosen to enable the energy transfer upconversion process (Figure 1a) leading to luminescence emissions in the green and red range of the electromagnetic spectrum, attractive for a broad variety of applications in biosensing and theranostics.^[54–56] For this, core-shell nanoparticles with high sensitizer and activator content were synthesized. Those UCNPs consist of β-NaYbF₄(20%Er) equipped with NaYF₄. Inspired by the approach of Cohen et al.,^[40] who used similar particles for low-irradiance imaging, those particles are referred to as alloyed UCNPs, whereas reference particles based on β-NaYF₄ doped with 20% Yb³⁺ and 2% Er³⁺ are titled as doped UCNPs (Figure 1b). The influence of nanoparticle size and the surface passivation effect depending on the shell material and shell thickness will be thoroughly discussed to give an insight into what parameters are important during particle design.

2. Results and Discussion

Enhancing the lanthanide content inside the UCNPs brings one obvious advantage in contrast to low-doped UCNPs: the high number of sensitizer ions is accompanied by a higher

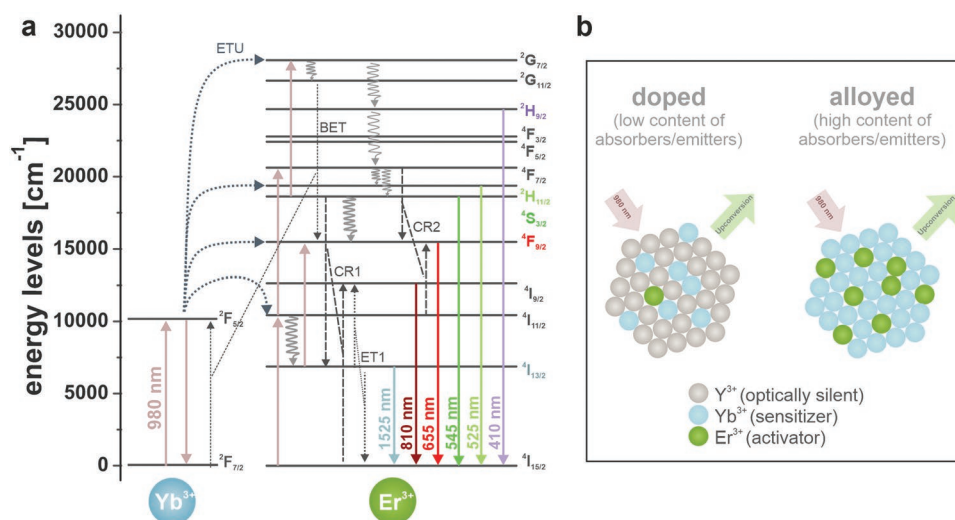


Figure 1. a) Energy level diagram of Yb³⁺ and Er³⁺ ions inside an upconversion nanocrystal. Wavenumbers of the electronic states are from Reference.^[57] ETU: energy transfer upconversion, BET: back energy transfer, and CR: cross relaxations. Curly arrows indicate non-radiative decay processes. b) Schematic representation of nanocrystals with high lanthanide content versus low lanthanide content (alloyed vs doped).

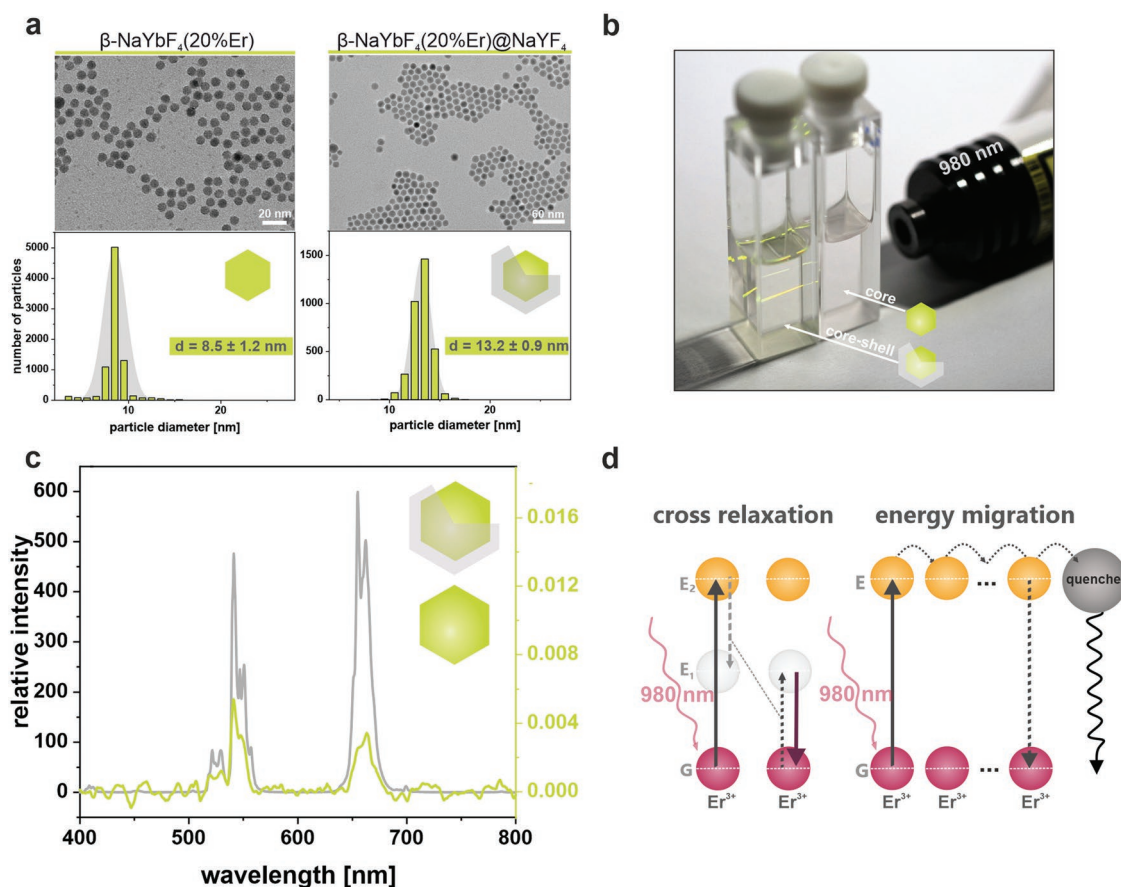


Figure 2. a) Transmission electron microscopy (TEM) micrographs of alloyed core ($\beta\text{-NaYbF}_4(20\%\text{Er})$) and core-shell ($\beta\text{-NaYbF}_4(20\%\text{Er})@\text{NaYF}_4$) particles with corresponding size histograms. b) Alloyed core (right) and core-shell (left) particles dispersed in cyclohexane, illuminated with 980 nm laser (200 mW, cw) in quartz cuvettes. c) Luminescence comparison of core and core-shell particles at 980 nm irradiation with 140 W cm^{-2} , spectra are normalized to particle concentration [particles mL^{-1}] and measured in cyclohexane. d) Schema of cross-relaxation and energy migration processes between lanthanide ions.

absorption of the excitation light. Comparing small alloyed $\beta\text{-NaYbF}_4(20\%\text{Er})$ (diameter: $8.5 \pm 1.2 \text{ nm}$, Figure 2a) and doped $\beta\text{-NaYF}_4(20\%\text{Yb},20\%\text{Er})$ (diameter: $7.6 \pm 1.2 \text{ nm}$, Figure S5, Supporting Information) nanoparticles, one finds absorption cross-sections about six times higher for alloyed compared to doped particles (Figure S1a, Supporting Information). The slightly larger alloyed particles contain about 5.6 times more Yb^{3+} ions, and 14 times more Er^{3+} ions, which are both capable of absorbing 976 nm light. Since the absorption coefficient of Yb^{3+} is one order of magnitude higher compared to Er^{3+} at 976 nm, the amount of sensitizer is mainly responsible for the difference.^[58] In contrast to the high absorption cross-section, upconversion luminescence (UCL) of alloyed UCNPs without a protective shell of NaYF_4 revealed a very low brightness (Figure 2b,c). The doped UCNPs, which have about six times less absorption cross-section, shows an about 50 times brighter UCL, which emphasizes that high absorption does not necessarily lead to high emission intensity. In contrast, after equipping the alloyed nanoparticles with an approximately 2 nm thin NaYF_4 shell a remarkable luminescence enhancement of a factor of $\approx 100\,000$ was found (integration between 400–750 nm).

The intense luminescence of the alloyed core-shell particles is contradictory to the concentration quenching theory, which says that cross-relaxations and energy migration between

lanthanide ions in proximity are responsible for low luminescence emissions (Figure 2d). The strong impact of surface passivation in core-shell systems on the luminescence intensity leads to the conclusion, that cross-relaxation cannot be the main reason for the low brightness of the core particles, as the shell has no influence on the cross-relaxation processes between the Er^{3+} ions. In contrast, the concept of energy migration between the lanthanide ions is very plausible: One ion in excited state can transfer the energy to a second ion in ground state, from where again energy is transferred to the next ion. In this way, energy migrates until the surface of the nanoparticle is reached, where surface quenching deactivates the excited lanthanide ion before the upconversion luminescence is emitted. In the case of core-shell architecture, the shell shields the particle from the environment and therefore inhibits the last step of energy transfer to quencher molecules, which enables the Er^{3+} ions to emit the upconversion luminescence.

Ytterbium as well as erbium ions are both enabling energy migration. In the alloyed particle system, the number of ions was significantly increased in contrast to conventional doped particles (factor 4 for Yb^{3+} , factor 10 for Er^{3+} for particles of the same size). Since the Yb^{3+} content is already high for doped particles (20%), it can be assumed that the Er^{3+} ions are mainly responsible for the enormous loss of energy for

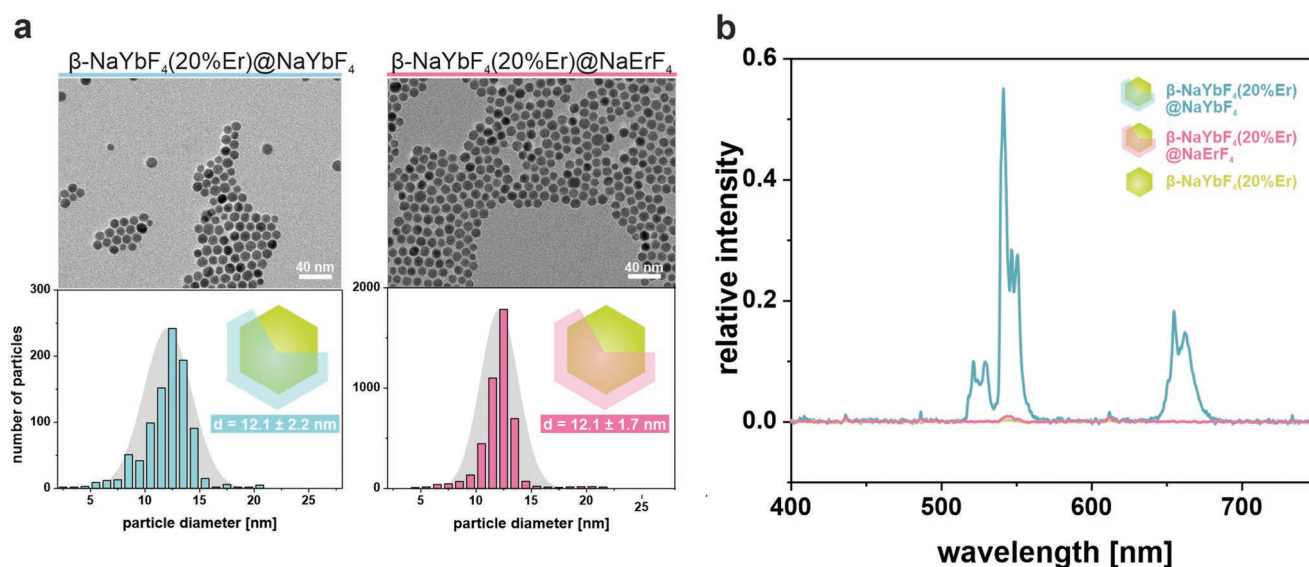


Figure 3. a) TEM micrographs of β -NaYbF₄(20%Er)@NaYbF₄ and β -NaYbF₄(20%Er)@NaErF₄ core-shell nanoparticles with corresponding size histograms. b) Luminescence of core and core-shell particles. Core particles are 8.5 ± 1.2 nm in diameter (see Figure 2a). Spectra are recorded at 980 nm excitation with 140 W cm^{-2} (cw) and normalized to particle concentration [particles mL⁻¹] in cyclohexane.

alloyed core-only systems. To prove this hypothesis, two core-shell structures have been synthesized: β -NaYbF₄(20%Er)@NaYbF₄ and β -NaYbF₄(20%Er)@NaErF₄ (Figure 3a). If one of the lanthanide ions in the shell does not favor energy migration brighter UCL will be expected, similar to the passivation effect known from NaYF₄ shells. The luminescence spectra of those particles and the corresponding core particles reveal the effect of the two kinds of shells (Figure 3b). An Er-shell has no significant effect on the luminescence since integration over the visible range (400–750 nm) led to an enhancement factor of 1.8 compared to the core particles, both very close to the noise. These results confirm that the Er³⁺ ions promote the energy to migrate through the shell without a barrier ending up in non-radiative deactivation at the particle surface or at crystal defects. Quenching effects by the solvent cannot explain the very low luminescence intensities of the Er-shelled particles, as a H/D exchange in the solvent leads only to an enhancement of approximately factor 5 (Figure S2a, Supporting Information). Therefore, quenching at crystal defects seems to be the more probable deactivation pathway. For the Yb³⁺ shell one would expect a luminescence enhancement independently from blocking energy migration, as about four times more Yb³⁺ ions are implemented into the particle, which would lead to an about four times higher absorption cross-section and therefore—in a simplified, ideal case—about four times higher luminescence. In fact, a strong luminescence enhancement by a factor of 51 was found for the Yb-shell. Surprisingly, the influence of non-radiative deactivation by C–H quenching of the solvent is comparable to the particles with NaErF₄ shell. The ²F_{5/2} level is not known to be influenced by C–H-vibrations,^[35] but a H/D exchange in the solvent leads to an enhancement factor of 4.5, which can only be caused by quenching of Er-ions in the core (Figure S2b, Supporting Information). Even when the particles are dispersed in strong quenching media enabling non-radiative deactivation of the ²F_{5/2} level by O–H-vibrations,^[35] the

Yb-shelled particles still show brighter luminescence compared to Er-shelled particles in D₂O (Figure S2c, Supporting Information). The fact that the Yb-shelled particles are still brighter in a high-quenching environment confirms our assumption that energy migration is more facilitated between Er³⁺ ions compared to Yb³⁺ ions, which is why the Yb-shell functions also as surface passivator here. A saturation of Yb ions, which also can suppress energy migration, can be excluded as the power-dependent luminescence tends not to flatten out at the excitation power at 140 W cm^{-2} (Figure S2d, Supporting Information).

However, as a NaYF₄ shell of similar thickness leads to an enhancement factor of about 100 000 (Figure 2c) it becomes obvious that the Yb-shielding cannot compete with growing an inert shell despite the higher absorption cross-section.

For a better understanding of the role of Yb³⁺ and Er³⁺ in the process of energy migration and quenching, four-particle systems of almost identical sizes with different percentages of Yb³⁺ and Er³⁺ doping have been compared: (80:2, 20:20, 20:2, and alloyed: 80:20). They were all equipped with a ≈ 1 nm NaYF₄ shell (TEM micrographs in Figure S3, Supporting Information). The particles with 80% Yb³⁺ should profit from the higher absorption cross-section, while particles with 20% Er³⁺ suffer from stronger energy migration to the particle surface, which is to a certain extent prevented by the NaYF₄ shell. Luminescence measurements (Figure S4, Supporting Information) revealed that the total intensity in the visible range is comparable for particles with 20%Yb³⁺: 2%Er³⁺, 80%Yb³⁺: 20%Er³⁺, or 80%Yb³⁺: 2%Er³⁺, with green-to-red ratio changing from 6.7 to 2.5 to 0.9 for those particles. The stronger green emission of the 80%Yb³⁺, 20%Er³⁺ particles probably results from the increased number of emitting ions, which is tenfold higher compared to particles with 80%Yb, 2%Er. As the higher Er³⁺ rate also leads to more C–H quenching, which mainly affects the red emission,^[59] the green-to-red ratio changes for those particles. The red emission is unexpectedly intense for both systems with

80% Yb³⁺ content and highest for the 80%Yb³⁺: 2%Er³⁺ system compared to 80%Yb³⁺: 20%Er³⁺. This is somehow surprising, since high amounts of Er³⁺ in the particle core are known for small green-to-red ratios.^[34,50] Apparently, high Yb³⁺ content also encourages the population of the red-emitting level, which can be explained with the back-energy-transfer (BET) process (Figure 1a). After absorption of three photons, energy can be transferred from Er³⁺ to Yb³⁺, ending up in the ⁴F_{9/2} level, where the red emission emerges.^[60] The more Yb³⁺ are surrounding one Er³⁺ ion, the higher is the probability for this process. According to the theory that Er³⁺ facilitates energy migration, stronger quenching effects for the particles with 20% Er³⁺ were expected.

The UCL of the 20%Yb³⁺: 20%Er³⁺ particles proves this assumption, as its intensity is much weaker at a green-to-red ratio of 3.5, compared to the 20%Yb³⁺: 2%Er³⁺ particles (Figure S4, Supporting Information). For the alloyed system, the two effects of enhanced absorption and enhanced energy migration are both contributing to the luminescence, which is why the total luminescence is similar compared to the doped system (20%Yb³⁺: 2%Er³⁺). Since the alloyed system is stronger influenced by energy migration and surface quenching, the degree of surface passivation shall be more important for this system. Shell growth of a 1 nm NaYF₄ shell is already improving the UCL efficiency. This leads to the question of to what extent an increasing shell thickness of shells prevents the migration.

Alloyed β -NaYbF₄(20%Er)@NaYF₄ particles with 8.5 nm core size and varying shell thicknesses were synthesized (Figure S5, Supporting Information). For comparison, also core-shell structures with doped composition in the core (β -NaYF₄(20%Yb,2%Er)@NaYF₄) were prepared (Figure S5, Supporting Information).

Since the alloyed particles are more influenced by energy migration and surface quenching, a stronger effect from shell growth was expected for those particles with high lanthanide content. This assumption was verified by the experimental data (Figure 4). The probably most special difference between alloyed and doped particles is the effect of the first, thin (1 nm) NaYF₄ shell. While for doped particles the difference in luminescence intensities between core-shell and core is about two orders of magnitude, the difference is about four orders of magnitude for alloyed nanoparticles (Figure S6a, Supporting Information). This means, already a thin shell is sufficient to block a large part of the energy transfer processes and therefore leads to an impressive enhancement of the luminescence intensities, which are then in a comparable range to the doped UCNPs. Surprisingly, further shell growth affects the green emission in a comparable way for alloyed and doped particles, while the red emission undergoes a significant increase of intensity. The strong enhancement of the red emission for alloyed particles with increased shell thickness is also reflected in the green-to-red ratio, which is >1 for core particles and particles with 1 nm

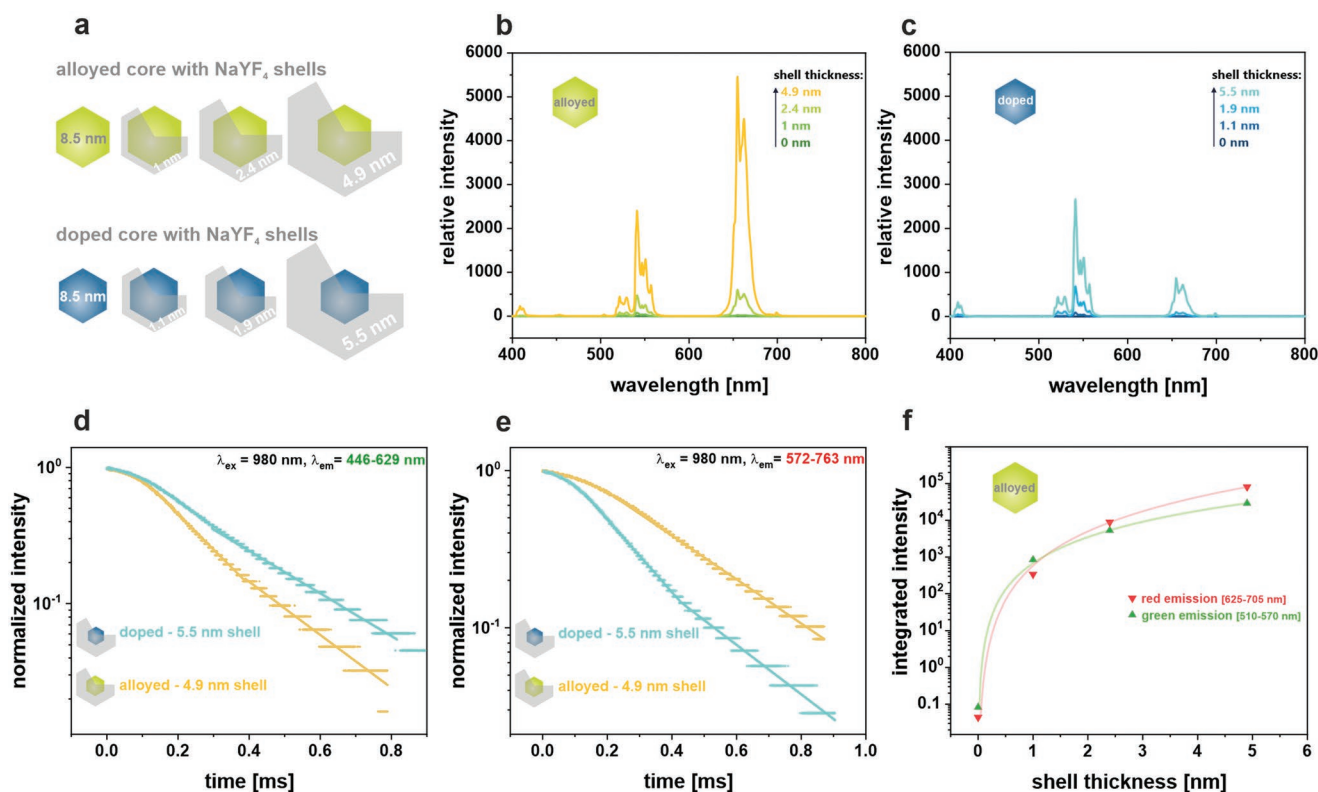


Figure 4. a) Scheme of core-shell structures with different thicknesses of NaYF₄ shells. Luminescence spectra of b) alloyed β -NaYbF₄(20%Er)@NaYF₄ and c) doped β -NaYF₄(20%Yb,2%Er)@NaYF₄ core-shell structures with varying shell thicknesses. Luminescence decay of d) green and e) red up-conversion emissions of alloyed and doped core-shell particles. f) Integrated luminescence intensities of green and red emissions of alloyed core-shell structures as a function of the shell thicknesses. Luminescence spectra were recorded in cyclohexane upon 980 nm excitation with 140 W cm⁻² (cw) and normalized to the particle concentration.

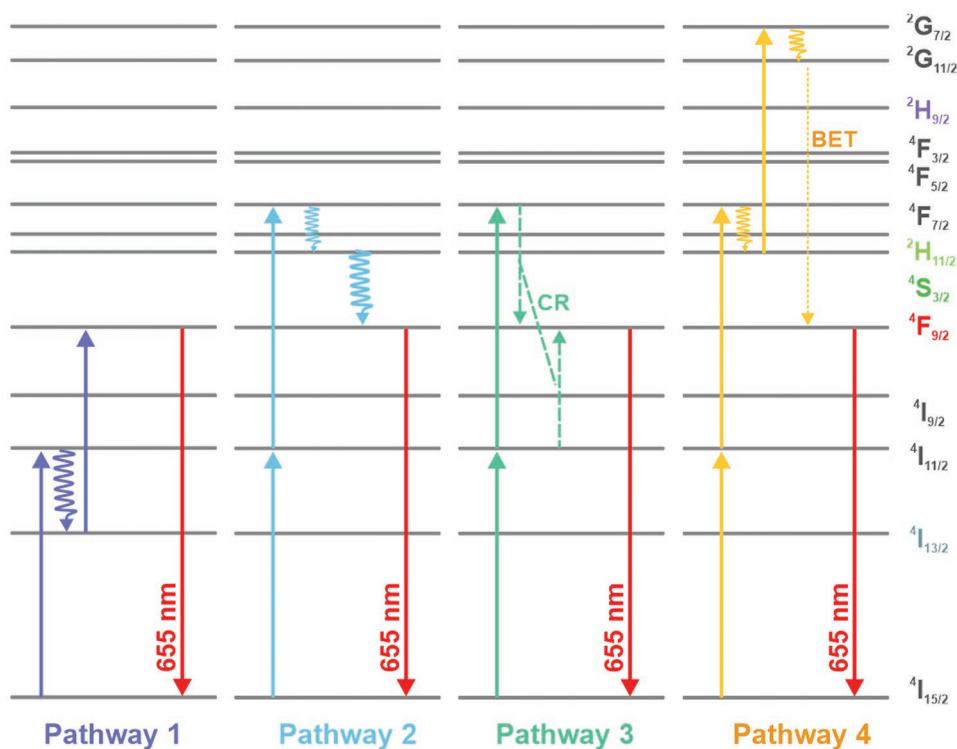


Figure 5. Excitation pathways for red upconversion luminescence. BET: back-energy-transfer and CR: cross-relaxations. Curled arrows indicate non-radiative decay processes.

shell, while it changes in favor of the red emission (<1) for thicker shells (Figure 4f). For doped particles, this remarkable change in peak ratios with increasing surface passivation was not observed (Figure S7, Supporting Information).

Alloyed nanoparticles in general have a much stronger red luminescence compared to doped nanoparticles. To understand this phenomenon, one has to review the processes which feed the red-emitting $^4F_{9/2}$ level (Figure 5).^[60–62] While pathways 1 and 2 should happen more or less equally for both particle systems, pathways 3 and 4 are dominated by cross-relaxation and back-energy-transfer processes. The probability of cross-relaxations increases with rising Er^{3+} content, while back-energy-transfer—where energy is transferred back from Er^{3+} to Yb^{3+} —should be facilitated for higher Yb^{3+} content. As in alloyed nanocrystals sensitizer and activator ions are not separated by optical silent ions, one can assume that pathways 3 and 4 play a major role additionally to the popular pathways 1 and 2, which then leads to the intense red emission. According to this theory, the contribution of three-photon-excitation is also increased for alloyed particles compared to doped particles. This was confirmed by excitation power-dependent luminescence measurements (Figure S5b, Supporting Information).

The impressive difference in red luminescence for surface protected and unprotected UCNPs is an indication that quenching processes have a strong impact on the population of the red-emitting level ($^4F_{9/2}$) in alloyed UCNPs. Meijerink et al. have shown, that the $^4F_{9/2}$ level is quenched by aliphatic C–H vibrations, while the green emission is stronger influenced by aromatic C–H vibrations.^[59] With cyclohexane (twelve C–H bonds) as solvent and oleic acid (33 C–H-bonds)

as surface ligand, this is a reasonable explanation for the increase of the red UCL with rising shell thickness. To prove this theory, luminescence of alloyed particles with 1 and 4.9 nm shells were both compared with and without oleic acid ligand in cyclohexane and DMF (six C–H-bonds) (Figure S8, Supporting Information). The change in peak ratio was stronger for the thin shell (36%) compared for the thicker 4.9 nm shell (11%), which supports the hypothesis of the strong impact of the interface and the environment of a particle system in dispersions.

The large difference in population pathways of alloyed and doped systems also influences the luminescence lifetimes of the green ($^2H_{11/2}$ and $^4S_{3/2}$) and red ($^4F_{9/2}$) emitting states. The main parameter influencing the visible upconversion decay times is quenching of the $1 \mu m$ level, which is also the level where probably most of the energy migration occurs.^[63] In an ideal case, where the surface of the alloyed particles is perfectly protected and hence surface quenching is prevented, energy migration still takes place, but is not followed by quenching. This would lead to strong, but delayed luminescence, as it was also observed by Zhang et al., who found longer luminescence lifetimes for samples with increased energy migration pathways.^[64] The green levels are depopulated by cross-relaxation processes in particles with high Er^{3+} content, leading to shorter lifetimes. Luminescence decay curves were recorded for the core-shell variants with the thickest shell (Figure 4d,e). While doped particles possess a longer luminescence lifetime for the green-emitting states, the alloyed particles show a longer lifetime for the red-emitting state ($^4F_{9/2}$), which confirms the theory. For particles with thin shells, this

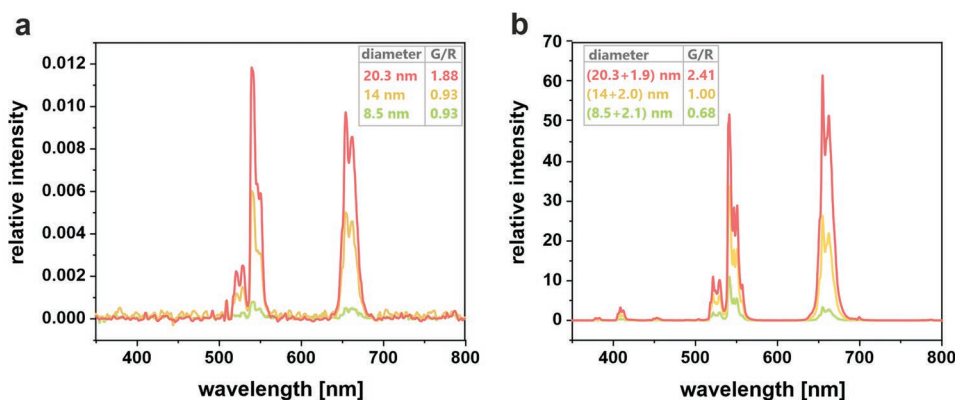


Figure 6. Upconversion luminescence spectra of alloyed a) core and b) corresponding core-shell particles with varying core diameters and constant shell thickness. Corresponding green-to-red ratios (G/R) of the integrated green and red luminescence emission are indicated in the legend. Measurements were performed in cyclohexane at 980 nm with an excitation power density of 140 W cm^{-2} . The spectra were normalized to the Er^{3+} concentration which was determined via ICP-OES.

effect is not as obvious, since the quenching processes of solvents and ligands play a greater role (Figure S9, Supporting Information).

Surface passivation is inevitable for alloyed nanoparticles to emit bright upconversion luminescence. The high lanthanide content favors energy migration which leads to quenching of excited state levels at the nanoparticle surface. According to this theory, surface processes are responsible for non-radiative energy loss. Since small nanoparticles have a higher surface-to-volume ratio compared to nanoparticles of larger diameter, alloyed core-shell UCNPs were synthesized with different core diameters to validate this fact (Figure S10, Supporting Information). An X-ray diffraction pattern of the largest core variant is displayed in Figure S11, Supporting Information, and proves the hexagonal crystal structure of the alloyed particles. For acquiring information from the UCL spectra of dispersions of particles of different size, doping, and concentration it is of greatest importance to carefully choose the method of data normalization. The informative value in normalizing to the particle concentration regarding the influence of surface-to-volume ratio is limited, as a larger particle just contains a higher number of absorbing and emitting ions, which is why higher luminescence intensities are recorded independently from the surface-to-volume ratio (Figure S12, Supporting Information). Hence, normalization to the concentration of Er^{3+} ions was performed (Figure 6), as this results in the relative emission intensity per emitting ion. In that respect, the largest particles are the brightest and show the longest decay times (Figure S13, Supporting Information), while the smallest nanoparticles show the lowest luminescence intensity and shortest lifetimes, which confirms the impact of the surface-to-volume ratio on the photophysical properties. From these results one can expect that shell growth is even more important for small particles with high surface-to-volume ratios, to prevent the quenching processes. Indeed, for small (8.5 nm) nanoparticles, the effect, comparing core to core-shell particles, is quite large (\approx factor 12 000). For the bigger (20.3 nm) particles, an enhancement factor of only \approx 5800 was found, which is in accordance with the lower surface-to-volume ratio. Additionally, the different degrees of quenching not only affect the total luminescence

intensity but also the green-to-red ratio (Figure 6). As it was found for particles with varying shell thicknesses, the influence of C–H-quenching on the red emission is stronger compared to green, which is why the green-to-red ratio decreases with a larger diameter for core-only as well as for core-shell particles.

3. Conclusion

This study focuses on the two effects of high lanthanide content inside UCNPs affecting their photophysical properties: enhanced absorption cross-section on the one side and enhanced energy migration on the other side. To profit from the higher absorption cross-section of alloyed particles with 80% Yb and 20% Er content, it is inevitable to have control about the energy migration as otherwise huge losses in luminescence intensity were observed. Surface passivation by NaYF_4 shell growth was demonstrated as a very efficient way to enhance particle luminescence, where luminescence increases with rising shell thickness. Reduction of the surface-to-volume ratio by increasing the particle diameter also helps to increase the particle brightness. Interestingly, depending on size and shell thickness very different green-to-red-ratios can be achieved. The examination of the influence of particle diameter and shell thickness can also be a decision aid for particle design. If the size plays no roll at all, core particles as large as possible with a shell thickness as thick as possible will give the brightest luminescence. As most applications involve a size limitation one must weigh up whether to choose a small core particle with a thick shell or a large core particle with a thin shell. Nevertheless, our results suggest equipping alloyed UCNPs with a NaYF_4 shell of at least 2 nm thickness. As already demonstrated one can achieve bright UCL at low power in microscopy,^[40] or if one envisions to use those particles as a reporter in biosensing, a thin shell might be the best choice to improve FRET efficiencies. Hopefully, this work stimulates researchers to rethink the optimal composition of small colloidal dispersed UCNPs. Modeling of rate equations for alloyed UCNPs might be helpful to find the best combination in lanthanide content and thickness of a NaYF_4 shell.

For comparison, also particles with 20% Yb, 2% Er were synthesized, which have similar luminescence intensities for thin NaYF₄ shells, while a great increase in the red emission with a rising degree of surface passivation was only found for the alloyed system. The very intense red emission can be a great chance for new applications including UCNPs. Since scattering effects are about a factor two times lower for red compared to green visible light (for Rayleigh scattering, $\approx \lambda^{-4}$),^[65] highly doped or alloyed nanoparticles are very suitable for bioimaging applications. There is also a huge application potential in photodynamic therapy, as many photosensitizer dyes (e.g., porphyrines or cyanines) have their absorption maximum in the range of the red upconversion emission.^[66]

4. Experimental Section

Characterization: Transmission electron microscopy images (TEM) were recorded with a 120 kV CM12 microscope (Philips). Particle dispersions (1 mg mL⁻¹) were dropped on carbon-coated copper grids, several micrographs were recorded per sample and to reveal a particle-size distribution at least 1000 particles were analyzed using the software ImageJ. Lanthanide concentrations were determined using optical emission spectroscopy with inductively coupled plasma excitation (ICP-OES) with a SPECTROBLUE FMX36 instrument (SPECTRO). Details for the calibration and concentration determination can be found in the Supporting Information. X-ray powder diffraction patterns (XRD) were collected using an STOE STADI P diffractometer equipped with a Dectris Mythen 1K detector. Monochromatic Cu K_{α1} radiation ($\lambda = 1.54056 \text{ \AA}$) was used and the resolution of the patterns was 0.005° (2θ). For luminescence recording, a custom-built spectroscopic set-up was used, including a Qmini UV/VIS spectrometer with the corresponding software Waves (Broadcom) and in 90° configuration a 980 nm, 200 mW (cw) laser module (Picotronic). The luminescence curves were normalized to the particle concentration or the Er³⁺-concentration. Signal smoothing was performed for samples with very low luminescence signals, using percentile filtering or Savitzky–Golay filtering.^[67] Green-to-Red ratios were calculated by dividing the integral of the green emission [510–570 nm] by the integral of the red emission [625–705 nm]. Luminescence decay curves were recorded with a custom-built setup, which was equipped with a 980 nm 200 mW (cw) laser module (Picotronic) and an optical chopper (Thorlabs). To collect green and red upconversion signals, two filters with transmission at [446–629 nm] and [572–763 nm] were inserted. A photomultiplier (PreSens) was used for signal amplification, while the oscilloscope Voltcraft PLUS DSO 8204 (Conrad) was incorporated for signal analysis. Absorption spectra of the particle dispersions in cyclohexane were recorded with a Cary 50 Scan UV-Visible Spectrophotometer (Agilent).

Synthesis of Upconversion Nanoparticles: The synthesis of alloyed UCNPs was performed according to a protocol published by the group of Bruce Cohen^[40] with modifications. For a 10 mmol batch size of β -NaYbF₄(20%Er) nanoparticles, the lanthanide trichloride hexahydrates YbCl₃ 6H₂O (8 mmol) and ErCl₃ 6H₂O (2 mmol) were dissolved in methanol. Other particle compositions were prepared analogously using desired molar ratios of lanthanide ions. The solution was transferred into a three-necked round-bottom flask, oleic acid (82.5 mL) and octadecene (100 mL) were added and heated to 110 °C under nitrogen atmosphere. Solvent and crystal water were evaporated by applying vacuum for 1 h. After cooling to room temperature, sodium oleate (31.25 mmol), NH₄F (50 mmol), oleylamine (95 mmol), and octadecene (43.75 mL) were added. To reach different nanoparticle sizes, the amount of oleylamine and sodium oleate was varied (see Table S1, Supporting Information). Vacuum was applied for another 20 min followed by degassing the solution three times. Subsequently, the mixture was heated to 315 °C under reflux with a heating rate of 16 °C min⁻¹ before rapidly cooling to room temperature after 45 min. For smaller batch sizes the time at 315 °C was shortened

(for 1 mmol: 15 min). The nanoparticles were precipitated in a centrifuge tube by addition of excess ethanol, collected via centrifugation (3000 g, 5 min), and purified by redispersing in cyclohexane and precipitating with ethanol three times. Afterward, the particles were dispersed in cyclohexane, aggregates were removed via centrifugation (3000 g, 5 min), and the particle dispersion was stored at 8 °C.

Synthesis of Core-Shell Nanoparticles: A shell precursor consisting of cubic NaYF₄ was prepared first. For a 10 mmol batch size, YCl₃ 6H₂O (10 mmol) was dissolved in methanol. The solution was transferred into a three-necked round-bottom flask and oleic acid (80 mL) and octadecene (150 mL) were added. The mixture was heated to 160 °C under nitrogen flow before vacuum was applied for 30 min. After cooling to room temperature, NH₄F (4.0 mmol) and NaOH (2.5 mmol), which was dissolved in methanol, were added and the mixture was heated to 120 °C for 30 min followed by a heating step to reflux (about 240 °C) for 30 min. After cooling to room temperature, the cubic particles were purified as described for hexagonal particles.

For the growth of a 2.4 nm shell, a three-necked round-bottom flask containing hexagonal particles (0.5 mmol) dispersed in cyclohexane, oleic acid (2.5 mL), and octadecene (2.5 mL) was heated to 100 °C under nitrogen atmosphere. A second flask containing cubic precursor material (1.2 mmol), oleic acid (6 mL), and octadecene (6 mL) was also heated to the same temperature. After applying vacuum to both flasks for 30 min, the flask containing the core particles was heated to reflux (about 325 °C). During heating, 0.5 mL of shell precursor was injected into the core particles via a syringe. At 325 °C, after every 4 min, small portions of shell precursor were injected into the core particles, to obtain uniform shell formation. After the last injection, the dispersion was kept at 325 °C for another 4 min and subsequently cooled to room temperature. Purification of the core-shell particles was performed as described for the core particles. For the synthesis of other shell thicknesses, the core to shell-precursor material was varied and the corresponding amounts of oleic acid and octadecene adjusted (calculations are described in the Supporting Information).

Supporting Information

Supporting Information is available from the Wiley Online Library or from the author.

Acknowledgements

Open Access funding enabled and organized by Projekt DEAL.

Conflict of Interest

The authors declare no conflict of interest.

Data Availability Statement

The data that support the findings of this study are available from the corresponding author upon reasonable request.

Keywords

lanthanides, luminescence, nanoparticles, near-infrared, upconversion

Received: December 21, 2021

Revised: February 18, 2022

Published online:

- [1] J. Niu, Xu Wang, J. Lv, Y. Li, Bo Tang, *TrAC, Tends Anal. Chem.* **2014**, 58, 112.
- [2] S. F. Himmelstoß, T. Hirsch, *Methods Appl. Fluoresc.* **2019**, 7, 022002.
- [3] A. Steinegger, O. S. Wolfbeis, S. M. Borisov, *Chem. Rev.* **2020**, 120, 12357.
- [4] P. Das, A. Sedighi, U. J. Krull, *Anal. Chim. Acta* **2018**, 1041, 1.
- [5] A. M. Ibarra-Ruiz, D. C. Rodríguez Burbano, J. A. Capobianco, *Adv. Phys.: X* **2016**, 1, 194.
- [6] X. Wang, H. Chang, J. Xie, B. Zhao, B. Liu, S. Xu, W. Pei, Na Ren, L. Huang, W. Huang, *Coord. Chem. Rev.* **2014**, 273–274, 201.
- [7] G. Chen, H. Qiu, P. N. Prasad, X. Chen, *Chem. Rev.* **2014**, 114, 5161.
- [8] Y.-Q. Liu, L.-Y. Qin, H.-J. Li, Y.-X. Wang, R. Zhang, J.-M. Shi, J.-H. Wu, G.-X. Dong, P. Zhou, *Nanomedicine* **2021**, 16, 2207.
- [9] M. V. Dacosta, S. Doughan, Yi Han, U. J. Krull, *Anal. Chim. Acta* **2014**, 832, 1.
- [10] S. Diao, G. Hong, A. L. Antaris, J. L. Blackburn, K. Cheng, Z. Cheng, H. Dai, *Nano Res.* **2015**, 8, 3027.
- [11] G. Chen, J. Shen, T. Y. Ohulchanskyy, N. J. Patel, A. Kutikov, Z. Li, J. Song, R. K. Pandey, H. Ågren, P. N. Prasad, G. Han, *ACS Nano* **2012**, 6, 8280.
- [12] F. E. Auzel, *Proc. IEEE* **1973**, 61, 758.
- [13] K. W. Krämer, D. Biner, G. Frei, H. U. Güdel, M. P. Hehlen, S. R. Lüthi, *Chem. Mater.* **2004**, 16, 1244.
- [14] G. Liang, H. Wang, H. Shi, H. Wang, M. Zhu, A. Jing, J. Li, G. Li, *J. Nanobiotechnol.* **2020**, 18, 154.
- [15] L. M. Wiesholler, T. Hirsch, *Opt. Mater.* **2018**, 80, 253.
- [16] H. P. Paudel, L. Zhong, K. Bayat, M. F. Baroughi, S. Smith, C. Lin, C. Jiang, M. T. Berry, P. S. May, *J. Phys. Chem. C* **2011**, 115, 19028.
- [17] L. M. Wiesholler, C. Genslein, A. Schroter, T. Hirsch, *Anal. Chem.* **2018**, 90, 14247.
- [18] G. Chen, J. Damasco, H. Qiu, W. Shao, T. Y. Ohulchanskyy, R. R. Valiev, X. Wu, G. Han, Y. Wang, C. Yang, H. Ågren, P. N. Prasad, *Nano Lett.* **2015**, 15, 7400.
- [19] Y. Zhu, Y. Ji, Q. Chen, C. Wang, X. Lu, Y. Mei, P. Xu, L. Li, T. Tan, J. Wang, *J. Lumin.* **2018**, 194, 420.
- [20] C. Zhao, X. Kong, X. Liu, L. Tu, F. Wu, Y. Zhang, K. Liu, Q. Zeng, H. Zhang, *Nanoscale* **2013**, 5, 8084.
- [21] T. Cheng, R. Marin, A. Skripka, F. Vetrone, *J. Am. Chem. Soc.* **2018**, 140, 12890.
- [22] N. Estebanez, A. Cortés-Villena, J. Ferrera-González, M. González-Béjar, R. E. Galian, S. González-Carrero, J. Pérez-Prieto, *Adv. Funct. Mater.* **2020**, 30, 2003766.
- [23] S. Han, R. Deng, Q. Gu, L. Ni, U. Huynh, J. Zhang, Z. Yi, B. Zhao, H. Tamura, A. Pershin, H. Xu, Z. Huang, S. Ahmad, M. Abdi-Jalebi, A. Sadhanala, M. L. Tang, A. Bakulin, D. Beljonne, X. Liu, A. Rao, *Nature* **2020**, 587, 594.
- [24] C. Würth, S. Fischer, B. Grauel, A. P. Alivisatos, U. Resch-Genger, *J. Am. Chem. Soc.* **2018**, 140, 4922.
- [25] S. Fischer, N. D. Bronstein, J. K. Swabeck, E. M. Chan, A. P. Alivisatos, *Nano Lett.* **2016**, 16, 7241.
- [26] M. Haase, H. Schäfer, *Angew. Chem., Int. Ed. Engl.* **2011**, 50, 5808.
- [27] I. Hyppänen, N. Höysniemi, R. Arppe, M. Schäferling, T. Soukka, *J. Phys. Chem. C* **2017**, 121, 6924.
- [28] M. Kraft, C. Würth, V. Muhr, T. Hirsch, U. Resch-Genger, *Nano Res.* **2018**, 11, 6360.
- [29] S. Wen, J. Zhou, K. Zheng, A. Bednarkiewicz, X. Liu, D. Jin, *Nat. Commun.* **2018**, 9, 2415.
- [30] J. Zhao, D. Jin, E. P. Schartner, Y. Lu, Y. Liu, A. V. Zvyagin, L. Zhang, J. M. Dawes, P. Xi, J. A. Piper, E. M. Goldys, T. M. Monro, *Nat. Nanotechnol.* **2013**, 8, 729.
- [31] D. J. Gargas, E. M. Chan, A. D. Ostrowski, S. Aloni, M. V. P. Altoe, E. S. Barnard, B. Sanii, J. J. Urban, D. J. Milliron, B. E. Cohen, P. J. Schuck, *Nat. Nanotechnol.* **2014**, 9, 300.
- [32] G. Chen, H. Ågren, T. Y. Ohulchanskyy, P. N. Prasad, *Chem. Soc. Rev.* **2015**, 44, 1680.
- [33] B. Shen, S. Cheng, Y. Gu, D. Ni, Y. Gao, Q. Su, W. Feng, F. Li, *Nanoscale* **2017**, 9, 1964.
- [34] N. J. J. Johnson, S. He, S. Diao, E. M. Chan, H. Dai, A. Almutairi, *J. Am. Chem. Soc.* **2017**, 139, 3275.
- [35] Z. Wang, A. Meijerink, *J. Phys. Chem. C* **2018**, 122, 26298.
- [36] W. Gao, Z. Sun, Q. Han, S. Han, X. Cheng, Y. Wang, X. Yan, J. Dong, *J. Alloys Compd.* **2021**, 857, 157578.
- [37] Q. Liu, Y. Zhang, C. S. Peng, T. Yang, L. -M. Joubert, S. Chu, *Nat. Photonics* **2018**, 12, 548.
- [38] B. Chen, W. Kong, N. Wang, G. Zhu, F. Wang, *Chem. Mater.* **2019**, 31, 4779.
- [39] Z. Meng, S. Zhang, S. Wu, *J. Lumin.* **2020**, 227, 117566.
- [40] B. Tian, A. Fernandez-Bravo, H. Najafabgdam, N. A. Torquato, M. V. P. Altoe, A. Teitelboim, C. A. Tajon, Y. Tian, N. J. Borys, E. S. Barnard, M. Anwar, E. M. Chan, P. J. Schuck, B. E. Cohen, *Nat. Commun.* **2018**, 9, 3082.
- [41] T. Förster, *Ann. Phys.* **1948**, 437, 55.
- [42] F. Wang, R. Deng, J. Wang, Q. Wang, Y. Han, H. Zhu, X. Chen, X. Liu, *Nat. Mater.* **2011**, 10, 968.
- [43] X. Chen, L. Jin, W. Kong, T. Sun, W. Zhang, X. Liu, J. Fan, S. F. Yu, F. Wang, *Nat. Commun.* **2016**, 7, 10304.
- [44] Q. Mei, A. Bansal, M. K. G. Jayakumar, Z. Zhang, J. Zhang, H. Huang, D. Yu, C. J. A. Ramachandra, D. J. Hausenloy, T. W. Soong, Y. Zhang, *Nat. Commun.* **2019**, 10, 4416.
- [45] L. Xu, Y. Liu, Z. Zhou, X. Sun, I. Ud Din, F. Khan, Y. Li, H. Li, J. Ren, J. J. Carvajal, J. Zhang, L. Liu, *Nanoscale* **2021**, 13, 9978.
- [46] B. Zhou, J. Huang, L. Yan, X. Liu, N. Song, L. Tao, Q. Zhang, *Adv. Mater.* **2019**, 31, e1806308.
- [47] L. M. Wiesholler, F. Frenzel, B. Grauel, C. Würth, U. Resch-Genger, T. Hirsch, *Nanoscale* **2019**, 11, 13440.
- [48] J. Wang, R. Deng, M. A. Macdonald, B. Chen, J. Yuan, F. Wang, D. Chi, T. S. Andy Hor, P. Zhang, G. Liu, Yu Han, X. Liu, *Nat. Mater.* **2014**, 13, 157.
- [49] J. Zhou, C. Li, D. Li, X. Liu, Z. Mu, W. Gao, J. Qiu, R. Deng, *Nat. Commun.* **2020**, 11, 4297.
- [50] Q. Chen, X. Xie, B. Huang, L. Liang, S. Han, Z. Yi, Yu Wang, Y. Li, D. Fan, L. Huang, X. Liu, *Angew. Chem., Int. Ed. Engl.* **2017**, 56, 7605.
- [51] T. Sun, Y. Li, W. L. Ho, Qi Zhu, X. Chen, L. Jin, H. Zhu, B. Huang, J. Lin, B. E. Little, S. T. Chu, F. Wang, *Nat. Commun.* **2019**, 10, 1811.
- [52] Y. Shang, S. Hao, W. Lv, T. Chen, Li Tian, Z. Lei, C. Yang, *J. Mater. Chem. C* **2018**, 6, 3869.
- [53] S. Wilhelm, M. Kaiser, C. Würth, J. Heiland, C. Carrillo-Carrion, V. Muhr, O. S. Wolfbeis, W. J. Parak, U. Resch-Genger, T. Hirsch, *Nanoscale* **2015**, 7, 1403.
- [54] J. Yan, B. Li, P. Yang, J. Lin, Y. Dai, *Adv. Funct. Mater.* **2021**, 31, 2104325.
- [55] F. Ding, Y. Zhan, X. Lu, Y. Sun, *Chem. Sci.* **2018**, 9, 4370.
- [56] X. Wang, R. R. Valiev, T. Y. Ohulchanskyy, H. Ågren, C. Yang, G. Chen, *Chem. Soc. Rev.* **2017**, 46, 4150.
- [57] W. T. Carnall, H. Crosswhite, H. M. Crosswhite, *Energy level structure and transition probabilities in the spectra of the trivalent lanthanides in LaF₃*, Argonne National Laboratory, Argonne, IL **1978**, <https://doi.org/10.2172/6417825>.
- [58] C. Strohhofer, A. Polman, *Opt. Mater.* **2003**, 21, 705.
- [59] F. T. Rabouw, P. T. Prins, P. Villanueva-Delgado, M. Castelijns, R. G. Geitenbeek, A. Meijerink, *ACS Nano* **2018**, 12, 4812.
- [60] C. Würth, M. Kaiser, S. Wilhelm, B. Grauel, T. Hirsch, U. Resch-Genger, *Nanoscale* **2017**, 9, 4283.
- [61] M. T. Berry, P. S. May, *J. Phys. Chem. A* **2015**, 119, 9805.
- [62] C. Lee, H. Park, W. Kim, S. Park, *Phys. Chem. Chem. Phys.* **2019**, 21, 24026.
- [63] M. Y. Hossan, A. Hor, Q. Luu, S. J. Smith, P. S. May, M. T. Berry, *J. Phys. Chem. C* **2017**, 121, 16592.
- [64] J. Zuo, D. Sun, L. Tu, Y. Wu, Y. Cao, B. Xue, Y. Zhang, Y. Chang, X. Liu, X. Kong, W. J. Buma, E. J. Meijer, H. Zhang, *Angew. Chem., Int. Ed. Engl.* **2018**, 57, 3054.
- [65] S. L. Jacques, *Phys. Med. Biol.* **2013**, 58, R37.
- [66] A. Ormond, H. Freeman, *Materials* **2013**, 6, 817.
- [67] W. H. Press, S. A. Teukolsky, *Comput. Phys.* **1990**, 4, 669.